Ultrawideband Conical Log-Spiral Circularly Polarized Feed for Radio Astronomy

Ultra-wideband Conical Log-Spiral Circularly Polarized Feed for Radio Astronomy

Kerlos Atia Abdalmalak, *Student Member, IEEE,* Gabriel Santamaría Botello, Sergio Llorente-Romano, Alejandro Rivera-Lavado, Jonas Flygare, *Student Member, IEEE,* José Antonio López Fernández, José Manuel Serna Puente, Luis Emilio García-Castillo, *Member, IEEE,* Daniel Segovia-Vargas, *Member, IEEE,* Miroslav Pantaleev, and Luis Enrique García-Muñoz

***Abstract*—In order to meet the requirements of the new generation of radio telescopes, we have developed a new topology called DYQSA, which stands for DYson Quad-Spiral Array. The design exhibits dual circular polarization in contrast to dual linear polarization of state-of-the-art feeds. It covers the required ultra-wideband (UWB) from $2\,\mathrm{GHz}$ to $14\,\mathrm{GHz}$ with an almost constant and real input impedance which facilitates the design of the feeding structure and the Low Noise Amplifiers (LNAs). Different versions are investigated for enhancing feed performance, ensuring higher aperture efficiencies and mechanical stability. Simulation results of the reflector loaded by the proposed feed show an aperture efficiency of $65 \pm 5\%$ can be achieved with a noise antenna temperature around $14\,\mathrm{K}$ and a System Equivalent Flux Density (SEFD) of about $1300\,\mathrm{Jy}$, both averaged over the required bandwidth at zenith. Measurements of the single-element and the four-element feeds are presented. Comparisons with other state-of-the-art feeds are shown in terms of total aperture efficiencies, design adaptability to different reflectors, calibration signal injection, the required number of LNAs per feed, cost, and physical volume.**

***Index Terms*—Ultrawideband antennas; Dual-polarized antennas; Circular polarization; Reflector antenna feeds; Conical antennas; Log spiral antennas; DYson Quad-Spiral Array (DYQSA); Radio astronomy; Radio telescopes; Very Long Baseline Interferometry (VLBI); VLBI2010 Global Observing System (VGOS); 3-D printing.**

I. Introduction

VERY Long Baseline Interferometry (VLBI) [1] is one of the primary space geodesy techniques that has been used since mid-1979. Actually, it is the only technique that can realize the International Celestial Reference Frame (ICRF) [2]. It uses multiple radio telescopes located on the earth, such as the Yebes observatory one in Fig. 1.

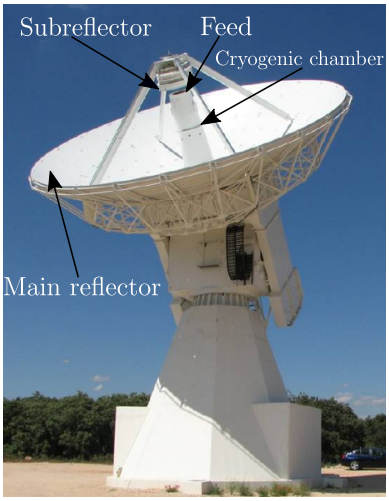

Fig. 1. The VGOS 13m radio telescope in Yebes, Spain.

These radio telescopes collect the very weak signals from far astronomical radio sources such as quasars, allowing the VLBI to estimate the inertial reference frame defined by such sources [3]. Simultaneously, by measuring the difference in the time of arrival of these signals to different radio telescopes, the relative positions of the antennas can be calculated. Since these antennas are fixed on the ground, their locations will track the instantaneous orientation of the earth.

The new observation system VLBI2010 Global Observing System (VGOS) [4] aims to improve VLBI data to meet the increasing demands. A broadband signal acquisition chain with fully digital electronics is needed for an expected position accuracy of about $1\,\mathrm{mm}$ [5]. For increasing sensitivity, VGOS requires a dual circularly polarized feed that covers an ultra-wideband frequency range from $2\,\mathrm{GHz}$ to $14\,\mathrm{GHz}$ with no need to compensate for the phase center changes via mechanical movement. The feed also needs to enable the reflector to have a System Equivalent Flux Density (SEFD) below 2500 Jansky (Jy) [6] for accomplishing acceptable Signal to Noise Ratio (SNR) values with reasonable integration times. This can be achieved by maximizing the total aperture efficiency and minimizing the noise contribution of the feed to the total system noise as will be discussed in Section II.

Manuscript received August 9, 2018. This work has been financially supported by CAM S2013/ICE-3004 "DIFRAGEOS", TEC2016-76997-C3-2-R, "DiDaCTIC": Desarrollo de un sistema de comunicaciones inalámbrico en rango THz integrado de alta tasa de datos, TEC2013-47753-C3, TEC2016-80386-P, and Comunidad de Madrid S2018/NMT-4333 MARTINLARA-CM projects.

Kerlos Atia Abdalmalak is with Signal Theory and Communication Department, Carlos III University of Madrid (UC3M), Spain and Electrical Engineering Department, Aswan University, Egypt (email: kerlos.atia@alumnos.uc3m.es).

Gabriel Santamaría Botello, Sergio Llorente-Romano, Luis Emilio García-Castillo, Daniel Segovia-Vargas, and Luis Enrique García-Muñoz are with Signal Theory and Communication Department, Carlos III University of Madrid (UC3M), Spain (email: legarcia@ing.uc3m.es).

Alejandro Rivera-Lavado is with Signal Theory and Communication Department, Carlos III University of Madrid (UC3M), Spain and Yebes Observatory, National Geographic Institute of Spain, Spain.

José Antonio López Fernández and José Manuel Serna Puente are with Yebes Observatory, National Geographic Institute of Spain, Spain.

Jonas Flygare and Miroslav Pantaleev are with Onsala Space Observatory, Chalmers University of Technology, Sweden.

TABLE I
MAIN PARAMETERS OF THE REFLECTOR

Parameter	Symbol	Value
Main reflector diameter	D_m	13200 mm
Main reflector focal length	F_m	3700 mm
Subreflector diameter	D_s	1550 mm
Half subtended angle	θ_e	65 deg
Parabola hole radius	ρ_{offset}	740 mm
Secondary focus position	L_p	3611.662 mm
Secondary focus to sub vertex	L_v	302.784 mm
Sub vertex position	L_s	3914.446 mm
Half flare main angle	Ψ	73.839 deg
Foci line tilt	φ	83.193 deg

Two main feed solutions are currently under consideration for the next generation of radio telescopes for VGOS applications: The Quadruple-Ridged Flared Horn (QRFH) [7] developed at the California Institute of Technology and the Eleven feed [8], [9] developed at Chalmers University of Technology. These two feeds have some deficiencies to be overcome [10], [11] as will be pointed out in Section V.

In this manuscript, a new feed for the VGOS radio telescope is presented. The rest of the manuscript is organized as follows: Section II discusses the reflector geometry with the calculations for SEFD and its different noise temperatures. Furthermore, this section analyzes the optimum performance of the VGOS radio telescope fed by an ideal Gaussian beam to have an upper limit estimation of the total system efficiency. The proposed topology including the design procedure to overcome the manufacturing challenges at such high frequencies of VGOS in addition to the full-wave electromagnetic simulations results for the feed-element are discussed in detail in Section III. Section IV shows the results of an isolated feed consisting of an array of spirals that enables dual circular polarization. Then, to prove the suitability of the proposed solution as a feed for VGOS radio telescope, an analysis of the reflector fed by DYQSA is presented in Section V. This analysis includes five main parameters: total radiation patterns, noise temperatures, directivity, aperture efficiency, and SEFD. Section VI presents comparisons between the proposed feed and the state-of-the-art ones. The measurement results of both the single element and the array feed are also shown in this section. Finally, conclusions are given in Section VII.

II. REFLECTOR ANTENNA

A. Reflector Antenna Geometry and Calculations

The main parameters of the reflector are summarized in Table I with a representation of its geometry in Fig. 2. It consists of one main parabolic mirror and a ring-focus subreflector. As can be seen from Table I, the reflector has a diameter of $13.2\,\text{m}$ while most of existing VLBI reflectors have significant larger diameters like Effelsberg radio telescope in Germany which has a diameter of $100\,\text{m}$. This compact size will significantly reduce the overall cost of the system.

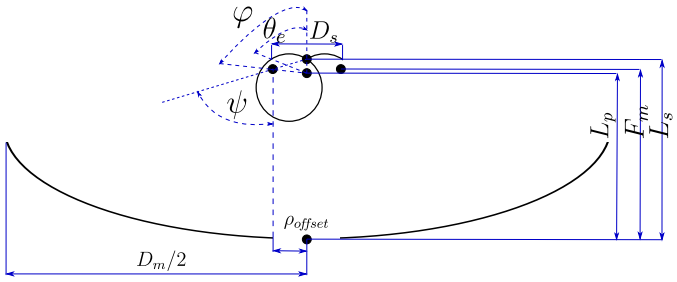

Fig. 2. Geometry of the VGOS reflector.

Moreover, such small reflectors can provide fast-slew speeds greater than $360\,\text{deg}/\text{min}$ allowing a larger number of observations, thus increasing the precision of the system. The feed is placed on the focal point of the reflector geometry, where it is cooled down to $15\,\text{K}$ inside the cryogenic receiver. The SNR of a radio telescope system based on continuous observations can be calculated using the following equation

$$\text{SNR} = \frac{S\sqrt{tB}}{\text{SEFD}} \tag{1}$$

where S is the flux density coming from the observed radio source in Jansky (Jy), while $1\,\text{Jy} = 10^{-26}\,\text{W}\,\text{m}^{-2}\,\text{Hz}^{-1}$, t is the integration time in seconds (s), B is the available bandwidth of the receiver system in hertz (Hz), SEFD includes the combined effect of antenna and all other noise sources into one parameter. Equation (1) shows that for a fixed incoming flux density and integration time, the SNR will be proportional to the square root of the bandwidth. Therefore, the ultra-wideband coverage for the receiver system (and therefore its feed) is critical. Also, for a fixed SNR, a lower SEFD yields a lower integration time. The SEFD can be calculated as

$$\text{SEFD} = \frac{2kT_{\text{sys}}}{A_{\text{eff}}} \tag{2}$$

where k is the Boltzmann constant, A_{eff} is the effective area of the reflector antenna and can be calculated from the total aperture efficiency of the reflector (η_{tot}) as $A_{\text{eff}} = \eta_{\text{tot}} A_{\text{phy}}$, where $A_{\text{phy}} = \pi\,(D_m/2)^2$ is the physical area of the reflector. Finally, T_{sys} is the equivalent system noise temperature which can be calculated as

$$T_{\text{sys}} = \eta_{\text{rad}} T_A + (1 - \eta_{\text{rad}})\, T_{\text{phy}} + T_{\text{REC}} \tag{3}$$

where η_{rad} is the antenna radiation efficiency, T_A is the antenna noise temperature including noise picked-up from the sky and the spill-over noise, T_{phy} is the physical temperature of the antenna, $(1 - \eta_{\text{rad}})\ T_{\text{phy}}$ is the noise temperature contribution from the feeds ohmic losses, and T_{REC} is the noise temperature of the complete receiver chain including the receiver components such as the cryogenic LNAs, coaxial cables, and calibration couplers. Using (3), the SEFD in (2) can be calculated as

$$\text{SEFD} = \frac{8k\,[\eta_{\text{rad}} T_A + (1 - \eta_{\text{rad}})\, T_{\text{phy}} + T_{\text{REC}}]}{\pi D_m^2 \eta_{\text{tot}}} \tag{4}$$

The above equation demonstrates the dependence of the SEFD (and hence SNR) on the feed selection which strongly affects both aperture efficiency and noise temperature of the reflector antenna. The calculation of the antenna noise temperature can be performed following [12] as

$$T_A = \frac{\int_0^{2\pi}\int_0^{\pi} F(\theta,\phi,f)T_b(\theta,\phi,f)\sin\theta\,\mathrm{d}\theta\,\mathrm{d}\phi}{\int_0^{2\pi}\int_0^{\pi} F(\theta,\phi,f)\sin\theta\,\mathrm{d}\theta\,\mathrm{d}\phi} \tag{5}$$

where $F(\theta,\phi,f)$ is the total power pattern of the reflector antenna which can be calculated using a combination of physical optics (PO) and physical theory of diffraction (PTD) with the simulation software TICRA GRASP [13] after exciting it by the proper feed. Parameters θ, ϕ, and f are the angle from the zenith (90-elevation angle), the azimuth angle, and the frequency respectively. $T_b(\theta,\phi,f)$ is the surrounding brightness temperature seen by the radio telescope calculated following [14] using the general brightness temperature model of the Square Kilometre Array (SKA) [15]. Once the noise temperature is calculated from (5), the spill-over noise temperature T_{sp} can be drawn from $T_A = T_{\mathrm{sky}} + T_{\mathrm{sp}}$ [16].

B. Reflector Antenna Fed by an Ideal Gaussian Feed

For comparison purposes through this manuscript, it is convenient to analyze the radiation patterns obtained for the radio telescope using an ideal Gaussian feed system. With this analysis, it is possible to have an upper limit estimation of the total aperture efficiency and directivity of the reflector system which are the key parameters for designing the proper feed [17]. To do this, an ideal Gaussian beam pattern is used as a feed. GRASP software has been used to analyze the whole reflector system at the desired range of frequencies from 2 GHz up to 14 GHz. For simplicity, results at 2 GHz, 8 GHz and 14 GHz are shown in Fig. 3. It shows perfectly symmetric radiation patterns as it is expected from the excitation with such symmetric beam. The directivity and aperture efficiency vs frequency of the reflector using this ideal Gaussian feed are shown in Fig. 4. It can be concluded that the expected directivity of the radio telescope varies from 47 dB to 65 dB. Also, this figure shows that the reflector has an almost flat efficiency of about 80% with a small degradation at lower frequencies.

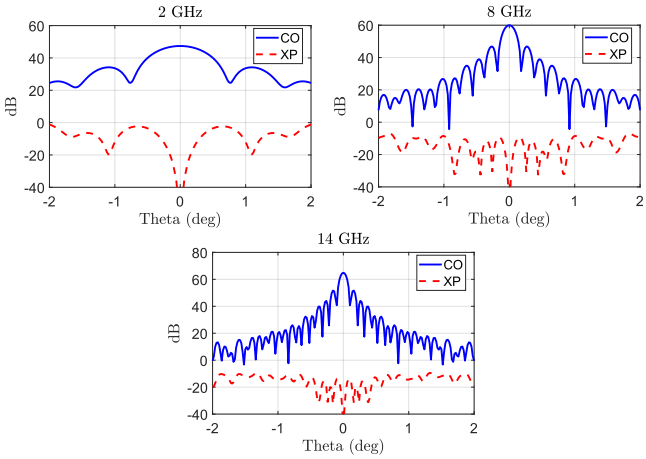

Fig. 3. Radiation patterns of the reflector fed by an ideal Gaussian feed.

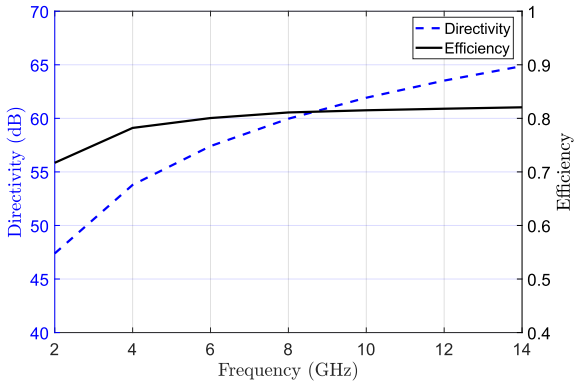

Fig. 4. Directivity and aperture efficiency of the reflector fed by an ideal Gaussian feed.

III. Conical Log-Spiral Antenna

The proposed solution is based on the self-complementary log-spiral antenna rounding a conical shape as shown in Fig. 5. This conical shape will provide unidirectional radiation patterns instead of the bidirectional ones typical for the planar spirals with avoiding the 3-dB loss characteristic in case of using the absorbing cavities. Recently, other solutions have included self-complementary structures able to cover large bandwidths such as the inverted conical sinuous antenna [18], [19] which is based on the projection of a sinuous pattern onto a cone placed above a ground plane. Although this solution exhibits stable radiation patterns, an almost fixed phase center, it has three main drawbacks for the application concerning this manuscript. Firstly, it provides linear polarizations so additional circuits or digital postprocessing techniques have to be added for linear-to-circular polarization conversion which has several disadvantages as will be discussed later in this section. Secondly, the addition of the ground plane affects its self-complementary nature and produces a frequency-dependent impedance. For example, in [18], the imaginary part of the impedance varies between 0 and $-300,\Omega$ over a relatively small bandwidth from 1 GHz to 3 GHz. This significantly increases the complexity of the LNA design and integration, especially for the required ultra-wideband range. Finally, the higher complexity of the manufacturing and assembly process for operation up to 14 GHz. The situation gets worse as the sinuous antenna has to be over-designed at the higher frequency to have stable properties at the high-frequency end [20]. Ongoing research is focusing on the optimization of the shape of the sinuous antenna and its manufacturing techniques to allow operation at higher frequencies [21].

The log-spiral antenna has four main geometrical parameters to control its electromagnetic features: the smallest diameter (d), the largest one (D), the spiral angle (α), and the conical angle (θ). Even though the conical log-spiral antenna has been proposed in the 20th century [22], to the best of the authors knowledge, no prototypes have been shown at the high frequencies required for VGOS (up to 14 GHz). This is due to the high manufacturing complexity and the stringent

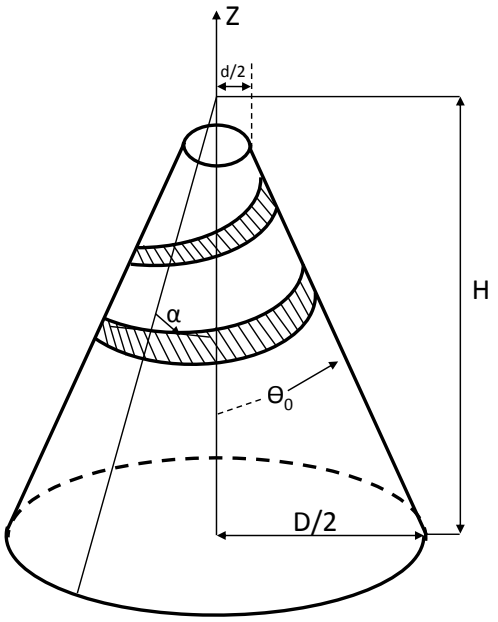

Fig. 5. Geometry of the Dyson conical log-spiral antenna.

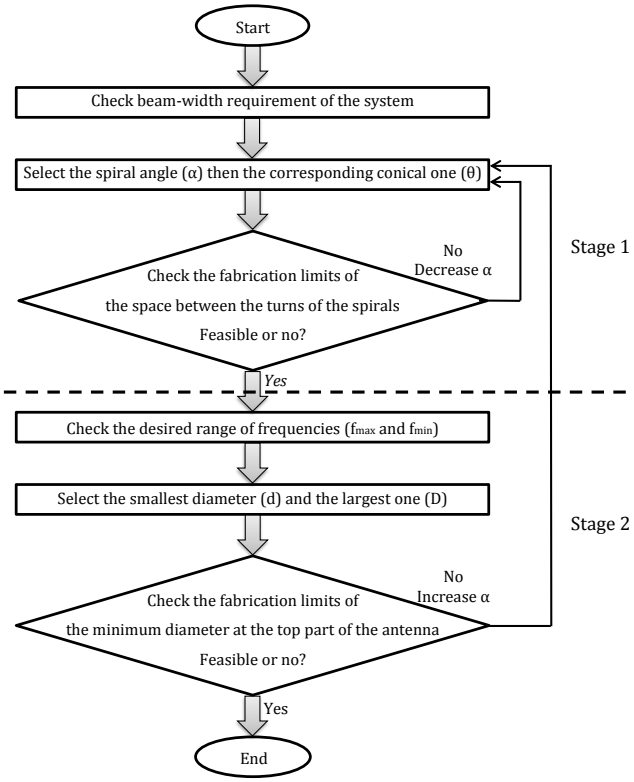

Fig. 6. The flowchart of the design procedure of the conical log-spiral antenna.

tolerance levels at the apex part. Figure 6 presents a systematic procedure for overcoming these design challenges. The design procedure mainly consists of two main stages: Firstly, the conical and spiral angles are selected. It is worth noting that lower values of the conical angles (θ) are more reasonable as they imply larger space between the arms of the spiral, which will facilitate the fabrication process. However, it will be shown that for our application (which requires high-frequency coverage), too small conical angles are not recommended as this will require a very small diameter at the top part of the cone (d) to cover up to 14 GHz.

Thus, the selection of the proper spiral angle (α) will be a tradeoff between the separation distance between the turns and the smallest diameter of the cone. Both represent the main fabrication challenges of this topology. The relation between beam widths and approximate directivity vs spiral angle (α) can be found in [23]. These relations are estimated for different conical angles (θ). After several optimization rounds, considering the requirements of VGOS, we select $\alpha = 85°$ which corresponds with a conical angle $\theta = 10°$

The second stage of the design process involves the selection of the smallest (d) and the largest diameters (D) of the cone. These two parameters control the maximum and the minimum working frequencies respectively. From the study of the relation between the smallest radius ($d/2$) vs the largest one ($D/2$) for different spiral (α) and conical (θ) angles [23], it can be observed that the smallest radius ($d/2$) is proportional to the conical angle (θ). This confirms the previous statement that a low conical angle will result in a small radius at the vertex of the cone, which will require a more complex fabrication process to cover the desired higher band. Considering VGOS system that requires covering a bandwidth from 2 GHz up to 14 GHz, $d = 3.2$ mm and $D = 60$ mm are good candidates.

The simulated radiation patterns of this log-spiral antenna

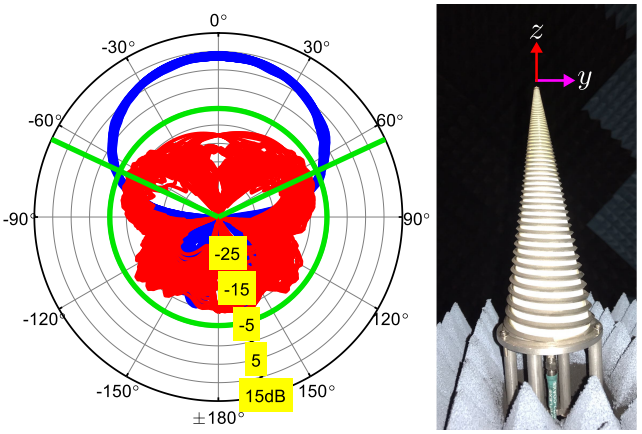

Fig. 7. Radiation patterns of the Dyson element.

using HFSS [24] are shown in Fig. 7 for the frequencies from 2 GHz to 14 GHz in steps of 2 GHz and for different cut planes from $\phi = 0°$ up to $\phi = 180°$ in steps of 15°. The blue and the red lines represent the circular copolar and the circular cross-polar polarizations respectively. The green lines show the half subtended angle from the focus of the subreflector (θ_e) while the green circle represents the elliptical polarization with an axial ratio of 3 dB. Figure 7 evidences the revolution symmetry of the radiation patterns at all frequencies with a gain around 10 dBi and Co/Xp-ratio on axis greater than 20 dB. Figure 8 presents the real and imaginary parts of the input impedance of the antenna in solid-blue and dashed-green respectively. As expected for this self-complementary topology, the impedance

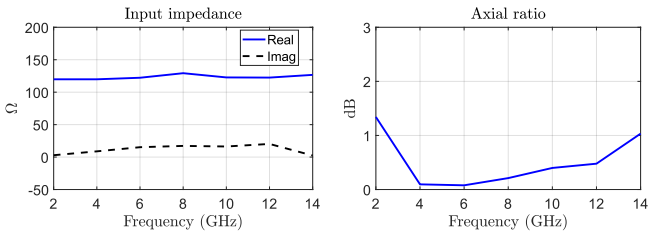

Fig. 8. Input impedance and axial ratio of the Dyson element.

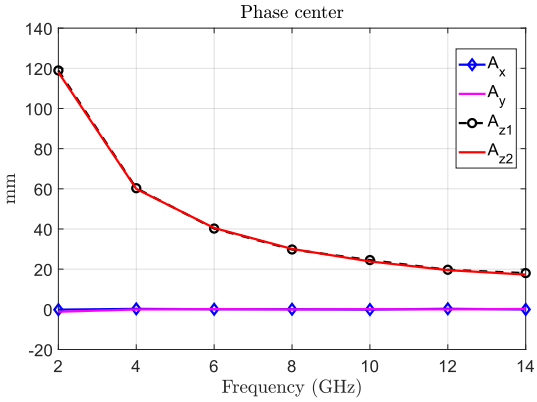

Fig. 9. Phase center estimation of the Dyson element.

is constant and almost real over the required frequency range. This is one of the main strong points of this solution as it will simplify the design of the LNA connected to the feed. Figure 8 also shows the axial ratio which is below 1.4 dB in the required band.

The phase center frequency dependence along the three axes estimated following [25] is presented in Fig. 9. A_x, A_y, and A_z are the x, y, and z coordinates of the phase center position respectively. The origin of the coordinate system for the phase center estimation is placed on the virtual apex of the cone (as in Fig. 7). A_{z1} and A_{z2} are the phase center calculated using two orthogonal cuts $\phi = 0°$ and $\phi = 90°$ respectively. All the phase centers have been calculated in the range of $\pm\theta_e$. Although the phase center is strongly shifted at lower frequencies which in general affects the total feed efficiency [26], it is possible to find an optimum position of the feed to get reasonable efficiency values as will be shown later in this section. Also, in the complete solution (considering the two circular polarizations) this issue is totally solved as it will be presented in the following section.

The total efficiency of the whole reflector using a specific feed can be factorized into four main subefficiencies which are spillover ($\eta_{\rm sp}$), polarization ($\eta_{\rm pol}$), illumination ($\eta_{\rm ill}$), and phase ($\eta_{\rm ph}$) subefficiencies. With such factorization, one may get an idea of the contribution of each subefficiency on the overall performance of the feed. These subefficiencies can be estimated by the integration of the feed's radiation patterns following [27], once they are calculated, the total aperture efficiency of the reflector using this feed can be calculated as $\eta_{\rm tot} = \eta_{\rm sp}\eta_{\rm pol}\eta_{\rm ill}\eta_{\rm ph}$. The subefficiencies and the total efficiency of the antenna when the Dyson element is used as the feed for the radio telescope are shown in Fig. 10. The

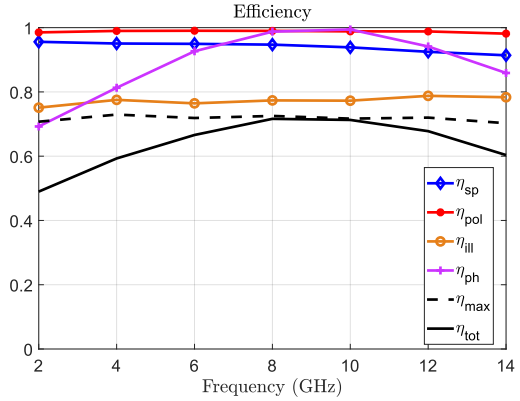

Fig. 10. Feed efficiency of the radio telescope based on the simulated radiation patterns of Dyson element.

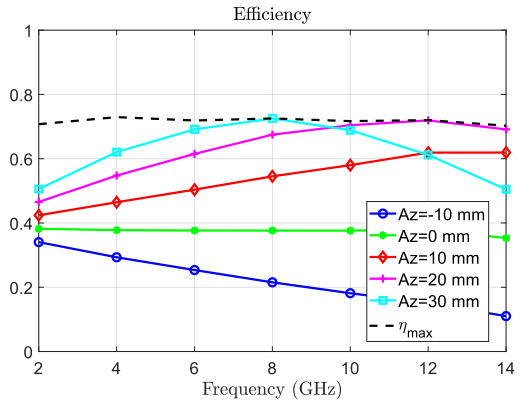

Fig. 11. Effect of the feed position on the aperture efficiencies.

dotted-black line is the total efficiency excluding the phase efficiency (which critically depends on the location of the feed). The frequency-averaged total efficiency has been maximized by studying its strong dependence on the displacement of the feed along the z-axis as shown in Fig. 11. The optimum performance is achieved when the virtual apex of the antenna is placed at 26 mm beyond the focus of the system.

The previous results demonstrate that the proposed antenna can be used as a broadband feed for the VGOS receiver. It exhibits circular polarization in contrast to the linear polarization as the state-of-the-art solutions. This could be potentially very useful as circular polarization is handled more simply for VLBI applications. Although circular polarization receivers can be built using linear-polarization feeds by the addition of linear-to-circular polarization conversion circuits like quarter-wave plates or other equivalent devices. This yields some drawbacks such as lower polarization purity and narrower effective bandwidth [28]. These are particularly relevant in the case of broadband receivers as most of these devices can provide a perfect 90 deg phase shift at only one or some frequencies, yielding phase errors away from these frequencies [29].

Another approach for the conversion from the linear polarization to the circular one is to reconstitute the circular polarization by recombining the signals after digitization. However,

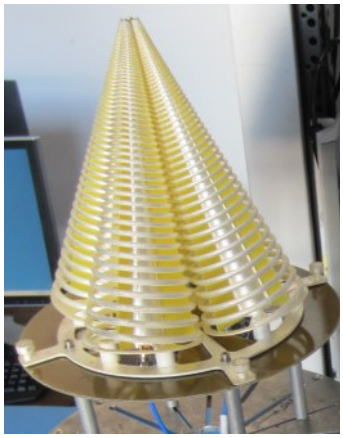

Fig. 12. Manufactured dielectric-free DYQSA version.

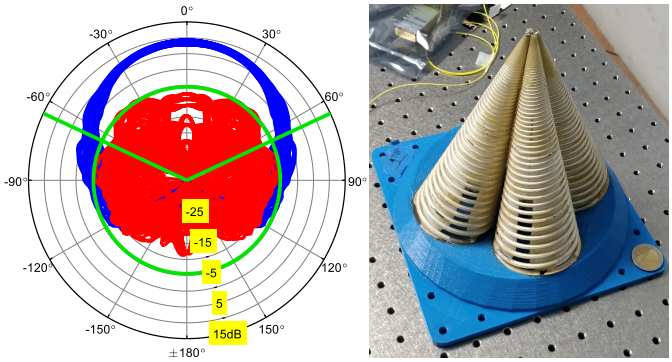

Fig. 13. Manufactured dielectric-filled DYQSA and its simulated radiation patterns.

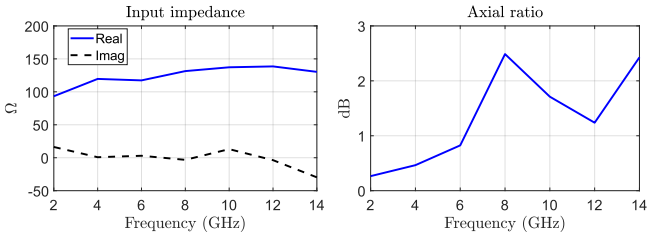

Fig. 14. Input impedance and axial ratio of the DYQSA feed.

it still needs a good calibration system to compensate phase and amplitude differences in the two paths which will increase the system complexity. On the other hand, for the proposed solution, we are providing a directly circular polarization feed without the need for either additional analog hardware or digital software. Moreover, the direct use of linear-polarization receivers will cause the loss of coherence between the different wide-separated stations in the network. This is because the linear dipoles will not remain parallel to each other, requiring tricky parallactic angle corrections compared to the simple phase correction in circular polarization.

IV. DYQSA Solution

To achieve dual-polarization as required by VGOS specifications, we use the implementation of an array with four elements of conical log-spiral antennas. In this design, each pair of antennas is devoted to a given polarization, one pair for the Right-Hand Circular Polarization (RHCP) and the other one for Left-Hand Circular Polarization (LHCP) as shown in Fig. 12. The reason why four antennas are used instead of two (one per polarization) is that in the latter case, the total radiation pattern of the radio telescope will be squinted: One polarization will be squinted to the left and the opposite for the other polarization, since the focus of the system is located close to the subreflector mirror. This effect is corrected by using two antennas per polarization.

The design has four differential ports that require eight single-ended LNAs (four per polarization). The addition of broadband baluns between the antennas and the LNAs will decrease the number of required single-ended LNAs from eight to four (two per polarization). An extensive study has been done to design the balun for these balanced antennas and its proper position. The first method is placing each balun inside its corresponding spiral antenna and shielding it with a metallic cone as shown in Fig. 12.

Although this excitation method is straightforward in its implementation, there is a high mutual coupling effect between the four metallic shields which significantly affects the radiation pattern stability over the required bandwidth. Thus, to enhance the electric properties of the system and reduce the effects of these metallic shielding, an updated version has been proposed. In this version, the four individual baluns have been replaced by one system of four baluns connected and introduced inside one metallic shielding through the center of the four spirals system. The balun is connected to the spiral using two bow-ties metallic patches at the apex of each spiral cone. The detailed discussion of this baluns-system has been reported in [30]. In spite of enhancing the electric properties of the solution in this new configuration by reducing the coupling between the metallic shielding and the antennas [31], the design still faces some mechanical issues arising from the low vibration tolerances of the system especially at the top part of the antenna. This affects the stability of the system and could cause short circuit problems at the element apices [32]. To overcome these mechanical issues, a new dielectric-filled DYQSA has been proposed.

In this third version, instead of manufacturing the antennas with a dielectric-free structure (as in Fig. 12), a low permittivity durable polyamide (nylon) material has been used for supporting the structure as shown in Fig. 13. Four thin supporting dielectric cones with a thickness of $1\,\mathrm{mm}$ are added as a support structure. This addition significantly enhances the robustness of the system against vibrations and increases the design stability. The simulated radiation patterns of this structure are presented in Fig. 13 covering the required bandwidth for different ϕ planes from $0°$ to $180°$ in steps of $15°$. Figure 13 shows a high-level of symmetry in the radiation patterns over the whole band. The maximum Co/Xp-ratio is above 15 dB with a constant gain of around 10 dBi.

Impedance and axial ratio of the array are presented in Fig. 14. These results confirm our predictions from the results of the single element with small deviations at higher frequencies. Figure 15 shows the phase center estimation of the whole array

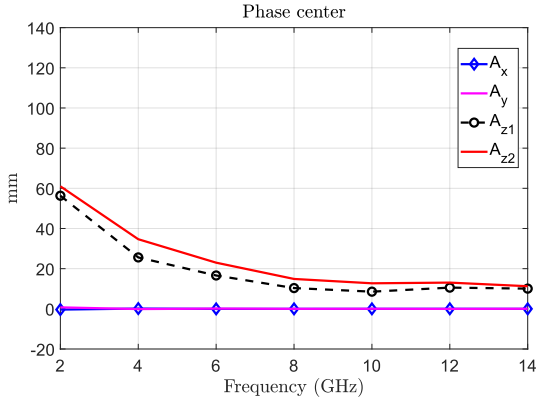

Fig. 15. Phase center estimation (in mm) of the DYQSA feed.

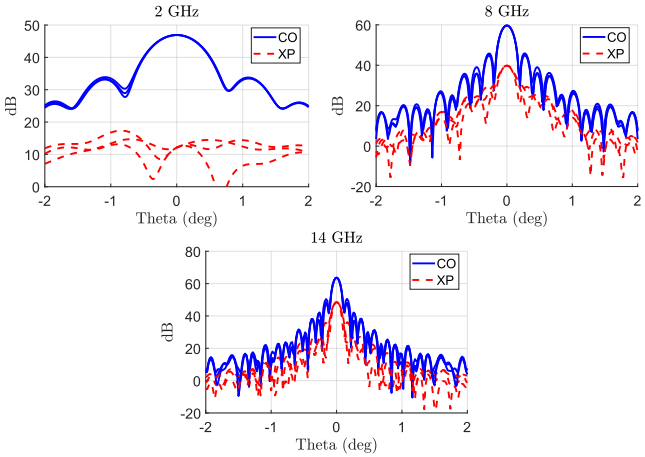

Fig. 16. Radiation patterns of the reflector fed by DYQSA for three cut planes $\phi = 0°$, $45°$ and $90°$.

when the origin of coordinates is placed on the virtual apex of the four cones. Although the phase center is not totally constant in the whole band, its variation in the 4 GHz - 14 GHz band is around two centimeters and three centimeters in the 2 GHz 4 GHz band. The overall variation is significantly lower than with the single Dyson element. In addition, in the next section, it will be shown that these small variations have negligible effects on the overall feed efficiency of the system.

V. Analysis of the Reflector Antenna Fed by DYQSA Solution

This section is dedicated to the results of the radiotelescope when using the four-element array as its feed. As presented in Section III, there is an optimum position of the feed. For this array system, the maximum total efficiency averaged over the frequency band (the optimum performance) is achieved when the apex of the array is placed 14 mm beyond the focus of the system. Radiation patterns of the radio telescope have been analyzed using GRASP software by introducing the radiation patterns of the array from HFSS as the feed of the radio telescope.

As it is common when designing feeds for reflectors such as in the case of QRFH [7] or Eleven [9], losses due to blockage and support structures are not included in the calculations

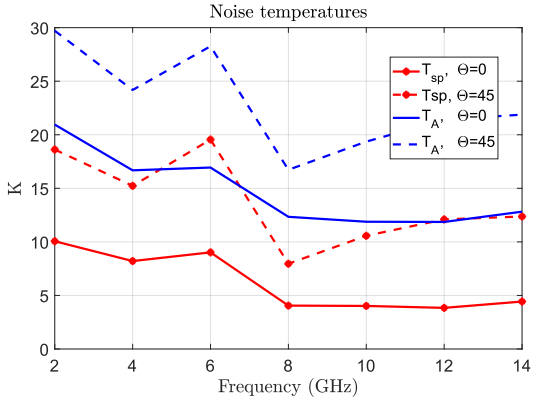

Fig. 17. Spill-over and antenna noise temperatures for the reflector fed by DYQSA.

as they are issues of the reflector itself instead of the feed. For simplicity, the results for 2 GHz, 8 GHz, and 14 GHz are shown in Fig. 16 for 3 cuts in planes $\phi = 0$ deg, 45 deg and 90 deg. Figure 16 demonstrates that the radio telescope fed by DYQSA has a high-level of symmetry in its radiation patterns over the required frequency range with a minimum Co/Xp-ratio level of 15 dB. Using the previous radiation patterns of the reflector in (5), the antenna noise temperature (T_A) along with the spill-over noise one ($T_{\rm sp}$) are shown in Fig. 17. The calculations have been done for two different cases. Firstly, at zenith $\theta = 0°$ (corresponding to an elevation angle of $90°$) when the reflector antenna is pointing vertically directly towards the sky and secondly, at a zenith angle of $45°$. The average spill-over noise and antenna noise temperatures over the whole band are 6 K and 14 K respectively at zenith. These average values increase by about 7 K at the lower elevation ($\theta = 45°$).

The directivity of the system versus the frequency has been estimated using GRASP and is plotted in Fig. 18. Considering all the previous results and the results presented in Section III, it can be concluded that the performance of the DYQSA is comparable with the optimum performance obtained using the ideal Gaussian feed (i.e. the difference in the directivity is below 1.2 dB). The aperture efficiencies for the radio telescope are shown in Fig. 19. It shows an almost constant total efficiency of around 65%. As expected from the phase center estimation of the array in Fig. 15, these variations have negligible effects on the total feed efficiency (the average phase efficiency over the required bandwidth is 97%).

The exact receiver noise temperature $T_{\rm REC}$ has not been measured yet as it needs further processing including the addition of the amplifiers and cooling down the receiver. However, it can be calculated from combining the noise temperatures for each source. Firstly, the cryogenic LNA proposed by Yebes observatory for VGOS reflectors has an almost flat measured noise temperature of 7.5 K in the operation band from 2 GHz to 14 GHz [30]. Secondly, following the estimations that have been done for QRFH [7], the other noise sources (calibration coupler and coaxial cables) will have a sum of noise temperatures of about 13 K, thus, the expected $T_{\rm REC}$ will be around 20 K. The noise contribution due to ohmic losses is 7 K per 0.1

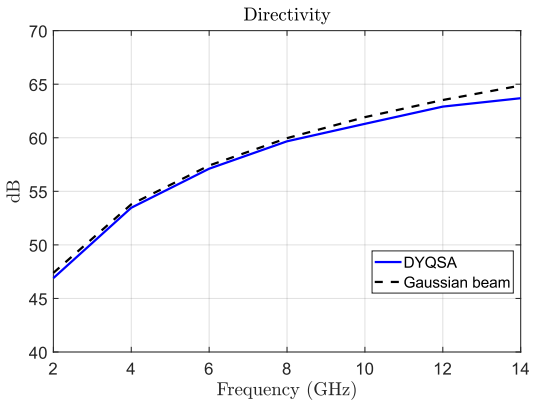

Fig. 18. Estimated directivity of the reflector from GRASP results.

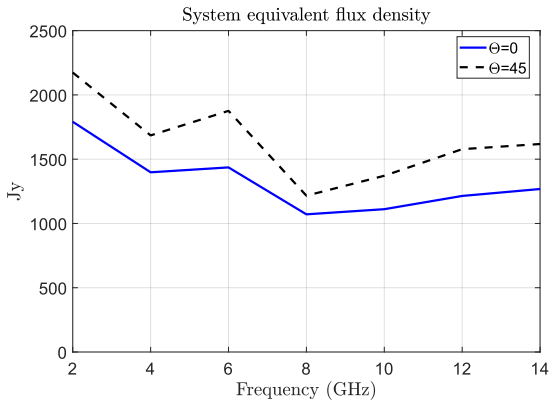

Fig. 20. Estimated SEFD of the reflector fed by DYQSA.

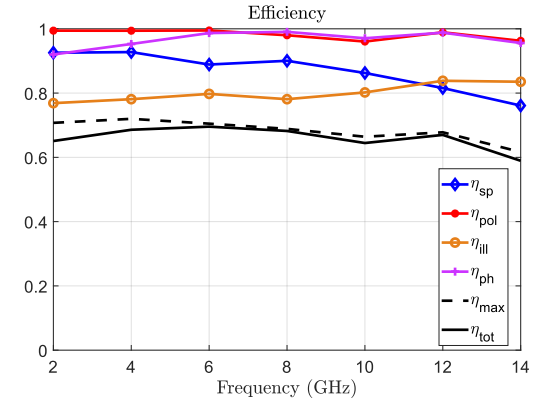

Fig. 19. Feed efficiency of the reflector based on the simulated radiation patterns of DYQSA.

dB loss at room temperature but as the feed will be cooled down to 15 K, this noise temperature will be smaller by a factor of 20 to be around 0.3 K per 0.1 dB loss. For DYQSA feed, the simulated radiation efficiency is around 0.9 (loss is less than 0.5 dB) which corresponds to 1.5 K of ohmic losses noise contribution. Hence, under the cryogenic cooling and for this radiation efficiency, the system noise temperature in (3) can be approximated as $T_{\rm sys} \approx T_A + T_{\rm REC}$.

Figure 20 presents the estimated SEFD of VGOS radio telescope based on DYQSA feed. A SEFD below 1800 Jy with an average of about 1300 Jy over the VGOS required bandwidth at zenith is shown. At a zenith angle of 45°, the average SEFD value is 1600 Jy which agrees with VGOS requirements. All these results demonstrate that the DYQSA solution is a potential feed candidate for VGOS radio telescopes.

VI. Comparison with the State-of-the-art Solutions and Measurements

A. Calibration Signal Injection

For comparison purposes, the calibration of the radio telescope is important. Generally, there are three main methods of calibration signal injection for VGOS feeds. Firstly, radiating the signal directly into the feed via a small transmitting probe. Secondly, coupling it into the signal chain after the LNA, or finally injecting it before the LNA (between the feed and LNA). However, due to the combining network and multiple LNAs needed for the DYQSA feed, it is not practical to use the last method. The Eleven feed solution [9] faces the same issue too.

B. LNAs Needed for the Feed & Feed Cost

To avoid noise degradation from the combining network, the LNAs can be directly connected to the balun. This will result in a total number of two LNAs per polarization or four LNAs per DYQSA feed which is half of the number of LNAs required by the Eleven feed. Also, the LNAs need to be matched within specified limits, otherwise, a degradation in the performance of the feed will occur. Even though the QRFH does not require any combining network (it has only one LNA per polarization), it still has degradation in the performance caused by the non-constant radiation patterns. Regarding the cost of the feeds, although DYQSA has the lowest cost (€8k) compared to the $33k and $15k of Eleven and QRFH feeds respectively [33], the low number of LNAs needed for QRFH (two per feed) makes it the lowest cost solution. Additionally, QRFH exhibits the lowest fabrication/assembly complexities. The overall cost of DYQSA, including the LNAs, is around 15% higher than QRFH (the cost of one LNA is around $5k) and less than half the cost of Eleven feed which has the highest number of LNAs per feed.

C. Design Adaptability of the Feed

Another key parameter for the comparison purposes is the adaptation easiness of the design, which ensures that the feed can be easily reoptimized to be used for several radio astronomy reflectors. While the QRFH design can be optimized to match different antenna optics, the Eleven feed has a fixed edge taper level of -10 dB at around 65° from its axis. Actually, the performance of the Eleven feed does not degrade significantly with small changes in the antenna optics. However, in the case of legacy International VLBI Service (IVS) antennas require an edge taper level of -10 dB at angles which are significantly different from 65°, the adaptability of the QRFH design will likely lead to better performance. From this point of view, DYQSA has the total ability to be

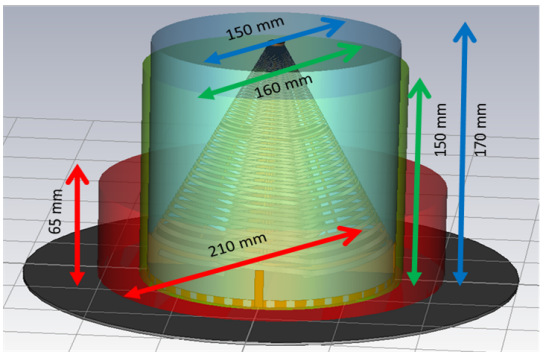

Fig. 21. Volumetric comparison of DYQSA (blue), Eleven (red) and QRFH (green) feed systems.

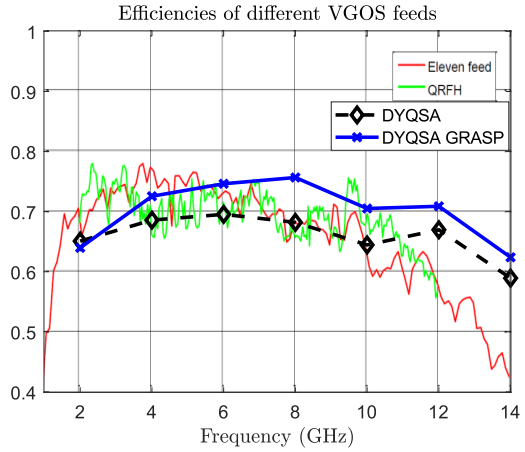

Fig. 22. Comparison of the efficiency of different feeds.

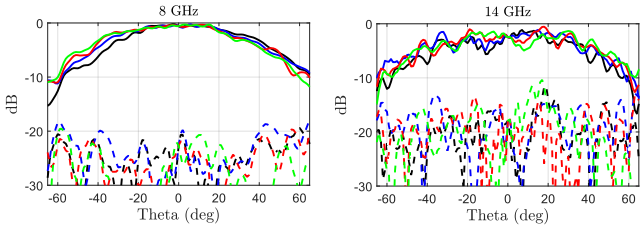

Fig. 23. Dyson element measured radiation patterns at 8 GHz and 14 GHz.

reconfigurable for a wide range of F_m/D_m ratios just like the QRFH as it has been shown in the design procedure of Section III that the beam width can be easily adjusted according to the requirements of the application.

D. Feed Volume

A volumetric comparison between DYQSA (in blue), Eleven (in red) and QRFH (in green) is shown in Fig. 21. This comparison shows that the size of the DYQSA is similar to that of the QRFH, and both have narrower-longer dimensions compared to the Eleven feed.

E. Feed Aperture Efficiency

A comparison between the three feeds from the aperture efficiency point of view is presented in Fig. 22. For the DYQSA feed, the efficiencies have been calculated using two different approaches. Firstly, using the closed-form equations following [27] in dotted-black line (the total efficiency in Fig. 19) and secondly using GRASP software in solid-blue line. For comparison purposes, the aperture efficiencies of both Eleven and QRFH feeds as they would perform in the VGOS reflector system [10], [33] are also shown in the same figure. The feed efficiency of the Eleven solution has been calculated using GRASP software at Onsala observatory while the QRFH efficiency calculation has been done using physical optics software at NASA Jet Propulsion Laboratory (JPL). The version of QRFH used in this comparison was designed for the frequency range from 2 GHz to 12 GHz so there are no available data for the comparison up to 14 GHz.

Figure 22 shows that DYQSA exhibits better performance than the other two solutions at higher frequencies, which show a linear degradation. Some recent work has been done for other different versions of QRFH feed for enhancing its properties and getting a flat performance over a wide bandwidth, for example by adding a dielectric spear [34]. However, it still has not been tested for the high frequencies required by VGOS. On the other hand, DYQSA shows a flat behavior which demonstrates that the phase center shifting is compensated. It can be seen from the estimation of the phase center (Section IV) as well as in the efficiency calculated in this section, that DYQSA shows an improvement in the global efficiency of the system due to the stability of the phase center. Also, from a general system perspective, and after connecting a feed to the LNAs, usually the SEFD suffers from an increase in the receiver noise temperatures at the high frequencies. From that perspective, the constant efficiency of the proposed solution at high frequencies is an attractive characteristic.

F. Single-Element and Array Measurements

The antenna has been manufactured in titanium following a 3-D printing growing technique [35] which becomes a promising technique especially for antennas at such frequency ranges where the sensitivity of the fabrication is critical [36]. Then, the solution is silver plated at the end of the process. In Fig. 23 and Fig. 24, the measured radiation patterns of single Dyson element and DYQSA feeds are plotted for different frequency points and for four different ϕ cuts. Both circular polarization components are plotted: RHCP (co-pol) in solid lines and LHCP (cross-pol) in dashed-ones.

The measurements for the single element have been done from 7 GHz to 14 GHz only as a proof of the concept. Although the single element provides a high-level of symmetry between the cuts in its measured radiation patterns with Co/Xp-ratio levels on axis greater than 15 dB, there is a reduction in the performance for the array version. The rest of this section is dedicated to analyzing the effect of this reduction on the whole reflector system and the possible causes of it.

Figure 25 presents the radiation patterns of the VGOS radio telescope when the DYQSA is used as the feed for cut planes $\phi = 0°, 45°$ and $90°$. They indicate the revolution symmetry of the radiation patterns with the Co/Xp-ratio level above 15 dB

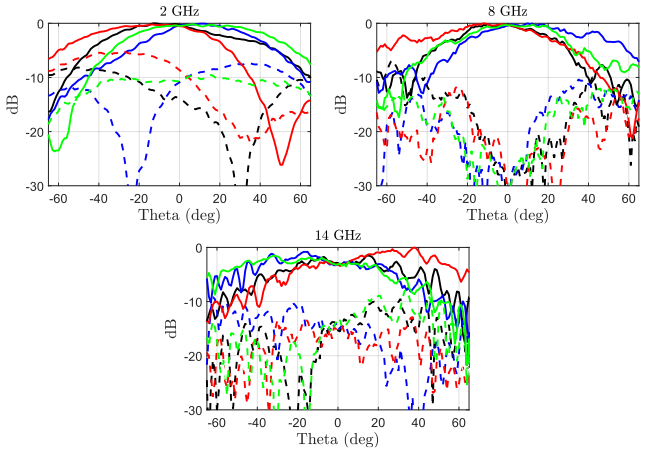

Fig. 24. DYQSA measured radiation patterns at 2 GHz, 8 GHz, and 14 GHz.

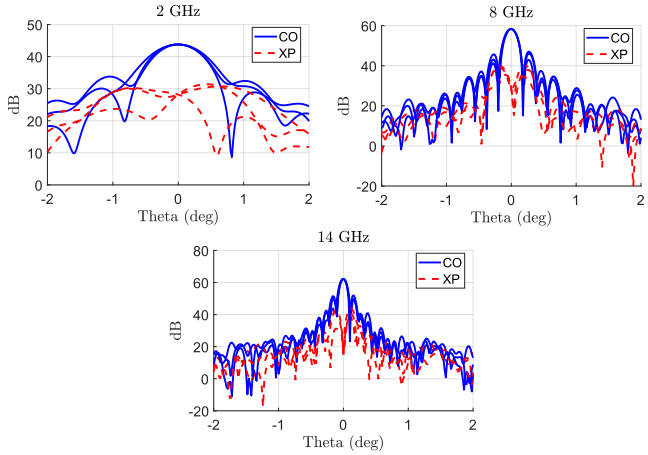

Fig. 25. Radiation patterns of the reflector based on the measured results of DYQSA feed (the ones on Fig. 24).

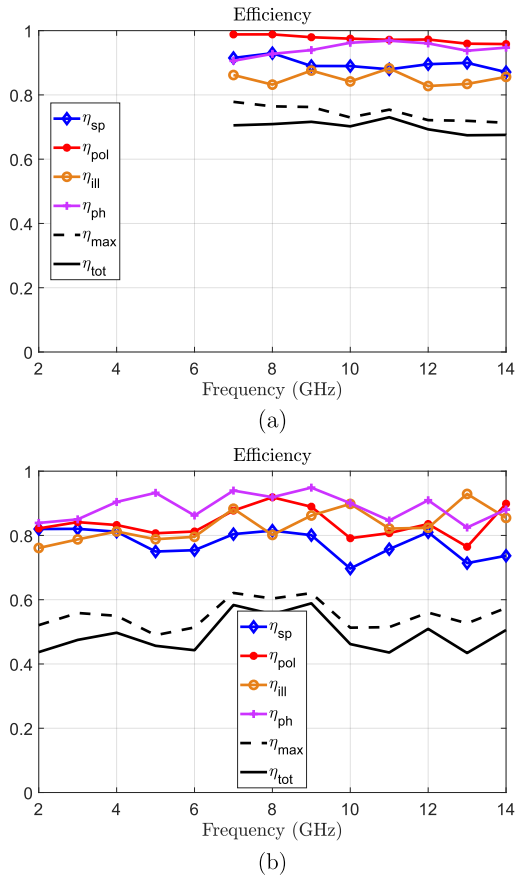

Fig. 26. Feed efficiency of the reflector based on the measured radiation patterns of (a) Dyson element and (b) DYQSA feed.

for the lower band and above 30 dB for the higher one which demonstrates that the small degradation of DYQSA radiation patterns does not significantly affect the overall radiation patterns of the reflector system. The feed efficiency estimation based on the measured radiation patterns is presented in Fig. 26, showing an almost flat performance. The total aperture efficiency is about 70% for the Dyson antenna for the band from 7 GHz to 14 GHz which is in excellent agreement with the simulated results. However, for DYQSA array, the average drops to about 50% over the required bandwidth contrary to the 65% obtained from the simulations.

Following measured results of the array element which show a great matching with the simulated ones, the degradation for DYQSA may be due to either the several assembly and disassembly processes for the same spirals in different versions and/or due to some misalignment issues. Especially that the misalignments between the elements will cause a phase mismatching between one turn of the spiral and its corresponding turn in the other antenna for the same polarization and this will affect the symmetry of the patterns. Further investigations need to be done in order to elucidate the reasons behind this degradation with ensuring higher alignment accuracy. Also, the antenna can be over-designed at the lower band (increase the largest diameter) to enhance the behavior of the feed at the lower frequencies. This will only increase the feed size and not its manufacturing/alignment complexity. Nevertheless, it is worth noting that these current results outperform the reported measurement results of the state-of-the-art feeds, especially at higher frequencies. For example, in the Eleven feed [9], the estimated efficiency based on the measured radiation patterns drops to about 30% at the higher frequencies.

VII. Conclusions

A new solution for covering the VGOS requirements has been proposed. It is based on a four-element array of conical log-spiral antennas. The proposed feed is adaptable to different antenna optics just like QRFH solution. It also provides two new attractive characteristics: dual circular polarization (in contrast to dual linear polarization present in the state-of-the-art feeds) and the constant and almost real input impedance of the antenna due to its self-complementary geometry, which beneficial for the LNA design. At a zenith angle of 45°, the proposed DYQSA solution is estimated to provide an average spill-over and antenna noise temperatures of about 13 K and 22 K respectively with a SEFD of about 1600 Jy and about 1300 Jy when the radio telescope points near the zenith. The total feed efficiencies of the proposed design and the two state-of-the-art solutions computed from the simulated radiation

patterns have been compared. This comparison demonstrates the frequency-independent behavior of DYQSA with an efficiency of $65 \pm 5\%$, contrary to the linear reduction in the efficiency of the other two solutions at high frequencies. The measurement results have a good level of agreement with the simulated ones, with an appreciable reduction in the DYQSA efficiency results. The average aperture efficiencies based on the measured radiation patterns for Dyson element are 70% for the frequencies range from 7 GHz to 14 GHz and 50% averaged over the entire band from 2 GHz to 14 GHz for DYQSA feed. These results show the potential of the DYQSA solution as a new VGOS feed.

ACKNOWLEDGMENT

The authors would like to thank Instituto Nacional de Técnica Aeroespacial (INTA) group for their help in the measurements, and Prof. Zoya Popovic at University of Colorado for her valuable discussion and comments. They would also like to thank the anonymous reviewers and associate editor for the constructive comments/suggestions.

REFERENCES

[1] H. Schuh and D. Behrend, "VLBI: A fascinating technique for geodesy and astrometry," *J. Geodyn.*, vol. 61, pp. 68–80, Oct. 2012.

[2] A. L. Fey *et al.*, "The second realization of the international celestial reference frame by very long baseline interferometry," *Astron. J.*, vol. 150, no. 2, p. 58, Jul. 2015.

[3] C. Ma *et al.*, "The International Celestial Reference Frame as Realized by Very Long Baseline Interferometry," *Astron. J.*, vol. 116, no. 1, pp. 516–546, Jul. 1998.

[4] W. T. Petrachenko *et al.*, "VLBI2010: Next Generation VLBI System for Geodesy and Astrometry," in *International Association of Geod. Symposia*, 2012, vol. 136, pp. 999–1005.

[5] H. Hase *et al.*, "The Emerging VGOS Network of the IVS," in *Proc. IVS 2012 General Meeting Proceedings*, no. September 2003, Madrid, Spain, 2012, pp. 8–12.

[6] B. Petrachenko, "Review of VLBI2010 Concept and General Specifications," in *Proc. IVS TecSpec Workshop*, Bad Kötzting, Germany, 2012.

[7] A. Akgiray, S. Weinreb, W. A. Imbriale, and C. Beaudoin, "Circular Quadruple-Ridged Flared Horn Achieving Near-Constant Beamwidth Over Multioctave Bandwidth: Design and Measurements," *IEEE Trans. Antennas Propag.*, vol. 61, no. 3, pp. 1099–1108, Mar. 2013.

[8] J. Yang, M. Pantaleev, P.-S. Kildal, and L. Helldner, "Design of Compact Dual-Polarized 1.210 GHz Eleven Feed for Decade Bandwidth Radio Telescopes," *IEEE Trans. Antennas Propag.*, vol. 60, no. 5, pp. 2210–2218, May 2012.

[9] J. Yang *et al.*, "Cryogenic 213 GHz Eleven Feed for Reflector Antennas in Future Wideband Radio Telescopes," *IEEE Trans. Antennas Propag.*, vol. 59, no. 6, pp. 1918–1934, Jun. 2011.

[10] B. Petrachenko, "VLBI2010 Feed Comparison," in *Proc. Int. VLBI Service Geod. Astrometry 2012 Annual Report, NASA/TP-2013-217511*, 2013, pp. 48–51.

[11] C. J. Beaudoin *et al.*, "A Cost and Complexity Survey on Emerging Technologies for the VGOS," in *Proc. Int. VLBI Service Geod. Astrometry 2014 General Meeting Proceedings: "VGOS: The New VLBI Network"*, K. L. A. Dirk Behrend, Karen D. Baver, Ed., Beijing, China, 2014, pp. 53–59.

[12] T. Y. Otoshi, *Noise temperature theory and applications for deep space communications antenna systems*. Artech House, 2008.

[13] "Ticra engineering consultants, GRASP," [Online]. Available: https://www.ticra.com/, Accessed: Mar. 20, 2019.

[14] J. Flygare *et al.*, "Sensitivity and Antenna Noise Temperature Analysis of the Feed System for the Onsala Twin Telescopes," in *23rd Eur. Very Long Baseline Interferom. Gr. Geod. Astrom. (EVGA)*, Goteborg, Sweden, 2017, pp. 10–14.

[15] G. Cortes-Medellin, "MEMO 95 Antenna noise temperature calculation," Tech. Rep., 2007.

[16] A. H. Akgiray, "New technologies driving decade-bandwidth radio astronomy : quad-ridged flared horn and compound-semiconductor LNAs," Doctoral dissertation, California Institute of Technology, Doctoral dissertation, 2013.

[17] B. Petrachenko *et al.*, "Design Aspects of the VLBI2010 System-Progress Report of the IVS VLBI2010 Committee," Tech. Rep., 2009.

[18] R. Gawande and R. Bradley, "Towards an Ultra Wideband Low Noise Active Sinuous Feed for Next Generation Radio Telescopes," *IEEE Trans. Antennas Propag.*, vol. 59, no. 6, pp. 1945–1953, Jun. 2011.

[19] R. S. Gawande and R. F. Bradley, "Characterization of the Active, Inverted, Conical Sinuous Antenna," in *Proc. XXIX Gen. Assemb. URSI*, Chicago, IL, 2008.

[20] R. S. Gawande, "Ambient and cryogenic, decade bandwidth, low noise receiving system for radio astronomy using sinuous antenna," Ph.D. dissertation, University of Virginia, Doctoral dissertation, 2011.

[21] N. Steenkamp, D. I. L. de Villiers, and N. Mutonkole, "Wideband pyramidal sinuous antenna for reflector antenna applications," in *Proc. 11th Eur. Conf. Antennas Propag. (EUCAP)*, Paris, France, Mar. 2017, pp. 2291–2295.

[22] J. Dyson, "The unidirectional equiangular spiral antenna," *IRE Trans. Antennas Propag.*, vol. 7, no. 4, pp. 329–334, Oct. 1959.

[23] J. Dyson, "The characteristics and design of the conical log-spiral antenna," *IEEE Trans. Antennas Propag.*, vol. 13, no. 4, pp. 488–499, Jul. 1965.

[24] "ANSYS Simulation driven product development, HFSS," [Online]. Available: https://www.ansys.com/, Accessed: Mar. 20, 2019.

[25] J.-p. Shang, De-min Fu, Ying-bo Deng, and Shuai Jiang, "Measurement of phase center for antenna with the method of moving reference point," in *Proc. 10th Int. Symp. Antennas Propag. EM Theory (ISAPE)*, Kunming, China, Nov. 2008, pp. 114–117.

[26] P.-S. Kildal, "Combined E-and H-plane phase centers of antenna feeds," *IEEE Trans. Antennas Propag.*, vol. 31, no. 1, pp. 199–202, Jan. 1983.

[27] P.-S. Kildal, "Factorization of the feed efficiency of paraboloids and Cassegrain antennas," *IEEE Trans. Antennas Propag.*, vol. 33, no. 8, pp. 903–908, Aug. 1985.

[28] I. Martí-Vidal, A. Roy, J. Conway, and A. J. Zensus, "Calibration of mixed-polarization interferometric observations-Tools for the reduction of interferometric data from elements with linear and circular polarization receivers," *Astron. Astrophys.*, vol. 587, p. A143, Mar. 2016.

[29] K. Das, "Conversion from linear to circular polarization in FPGA in real time," Ph.D. dissertation, Universität zu Köln, Doctoral dissertation, Jun. 2013.

[30] K. A. Abdalmalak *et al.*, "Radio astronomy ultra wideband receiver covering the 214 GHz frequency band for VGOS applications," in *Proc. 10th Eur. Conf. Antennas Propag. (EuCAP)*, Davos, Switzerland, Apr. 2016, pp. 1–5.

[31] K. A. Abdalmalak, S. L. Romano, L. E. G. Munoz, and D. S. Vargas, "Dual polarized ultra wideband feed system for VLBI global observation system applications," in *Proc. Global Symp. Millim. Waves (GSMM) & ESA Workshop Millimetre-Wave Technol. Appl.*, Espoo, Finland, Jun. 2016, pp. 1–4.

[32] K. A. Abdalmalak *et al.*, "An updated version of the Dyson Conical Quad-Spiral Array (DYQSA) feed system for VGOS applications," in *Proc. IEEE Int. Symp. Antennas Propag. & USNC/URSI Nat. Radio Sci. Meeting*, San Diego, CA, USA, Jul. 2017, pp. 1539–1540.

[33] M. Pantaleev *et al.*, "Broadband Feeds for VGOS," in *Proc. Int. VLBI Service for Geod. Astrometry 2014 General Meeting Proceedings: "VGOS: The New VLBI Network"*, D. Behrend, K. D. Baver, and K. L. Armstrong, Eds., Beijing, China, 2014, pp. 60–67.

[34] A. Dunning *et al.*, "An ultra-wideband dielectrically loaded quad-ridged feed horn for radio astronomy," in *Proc. IEEE-APS Topical Conf. Antennas Propag. Wireless Commun. (APWC)*, Turin, Italy, Sep. 2015, pp. 787–790.

[35] "3D Systems Manufacturing," [Online]. Available: https://www.3dsystems.com/, Accessed: Mar. 20, 2019.

[36] A. A. Althuwayb *et al.*, "3-D-printed dielectric resonator antenna arrays based on standing-wave feeding approach," *IEEE Antennas and Wireless Propagation Letters*, vol. 18, no. 10, pp. 2180–2183, Oct. 2019.